Ferrocene functionalized enantiomerically pure Schiff bases and their Zn(II) and Pd(II) complexes: a spectroscopic, crystallographic, electrochemical and computational investigation

Salvador Celedon, Paul Hamon, Vania Artigas, Mauricio Fuentealba, Samia Kahlal, David Carrillo, Jean-Yves Saillard, Jean-René Hamon, Carolina Manzur

Ferrocene functionalized enantiomerically pure Schiff bases and their Zn(II) and Pd(II) complexes : a spectroscopic, crystallographic, electrochemical and computational investigation†

Salvador Celedón,*[a,#] Paul Hamon,[b] Vania Artigas,[c] Mauricio Fuentealba,[c] Samia Kahlal,[b] David Carrillo,[a] Jean-Yves Saillard,[b] Jean-René Hamon*[b] and Carolina Manzur*[a]

[a] *Laboratorio de Química Inorgánica, Instituto de Química, Facultad de Ciencias, Pontificia Universidad Católica de Valparaíso, Avenida Universidad 330, Curauma, Valparaíso, Chile. E-mail: cecilia.manzur@pucv.cl*

[b] *Univ Rennes, CNRS, ISCR (Institut des Sciences Chimiques de Rennes) – UMR 6226, F-35000 Rennes, France. E-mail: jean-rene.hamon@univ-rennes1.fr*

[c] *Laboratorio de Cristalografía, Instituto de Química, Facultad de Ciencias, Pontificia Universidad Católica de Valparaíso, Avenida Universidad 330, Curauma, Valparaíso, Chile.*

[#] *Present address: Instituto de Ciencias Naturales, Universidad de las Américas, Manuel Montt 948, Santiago, Chile. E-mail: sceledp@edu.udla.cl*

† Electronic supplementary information (ESI) available: CCDC 2129661 and 2129662. For ESI and crystallographic data in CIF or other electronic format see DOI:

Abstract

In this contribution, we describe the synthesis, spectroscopic and structural characterization, as well as the electrochemical behavior of a series of four chiral ferrocene-functionalized Schiff base compounds derived from enantiomerically pure (1R,2R)-(−)-1,2-diaminocyclohexane. The ferrocene enaminones **3** and **4** were obtained upon monocondensation of ferrocenoylacetone Fc-C(=O)CH_2C(=O)R (R = CH_3, **1**; 4-C_6H_4OH, **2**; Fc = (η^5-C_5H_5)Fe(η^5-C_5H_4)) with one amino group of the primary diamine. The two bimetallic complexes **5** and **6** were prepared via a one-pot three-components template procedure involving half-unit **3**, 4-methoxysalicylaldehyde and tetrahydrated zinc(II) nitrate for **5**, and half-unit **4**, 4-formyl-3-hydroxybenzoic acid and palladium(II) acetate for **6**. All the syntheses were carried out in refluxing ethanol and compounds **3-6** were isolated as thermally stable, air and moisture compatible colored solids in 71-83% yields. They were characterized by several analytical (EA, ESI-MS) and spectroscopic methods (^{1}H/^{13}C NMR, FT-IR, UV-vis), including the molecular structures of **3** and **4** that were unequivocally established by single crystal X-ray diffraction analyses. Both crystallize in the orthorhombic non-centrosymmetric space group $P2_12_12_1$ with two (R,R)-(−)-chiral carbon atoms in the structures. Cyclic voltammetry showed that the greatest anodic shifts (270 mV) of the ferrocenyl Fe(II)/Fe(III) redox potentials is observed for the D-π-A push-pull derivative **6**. Beyond experimental characterization, DFT- and TDDFT-based theoretical analyses of the new chiral ferrocene-containing Schiff base complexes allow interpretation of their observed spectroscopic, structural and electronic features.

Introduction

Ferrocene [Fe(η^5-C_5H_5)$_2$] (FcH), the iconic organometallic complex discovered 70 years ago,[1-5] displays exceptional properties,[6] and research on ferrocene and its derivatives continues to demonstrate great interest and vitality.[7-9] Indeed, ferrocene is fascinating due to its stability under aerobic, moist and photochemical conditions, its thermodynamic robustness, its unique structural properties such as adequate rigidity and steric bulkiness, its easy derivatization,[10,11] and its remarkable redox properties,[3,12,13] endowing ferrocene and its derivatives numerous applications in a wide range of fields, including catalysis,[14] sensing,[15,16] batteries,[17] medicinal chemistry,[18-20] and teranostics.[21] Ferrocene has also been explored as an appealing building block in the construction of organometallic chromophores, including asymmetric multidentate ferrocene functionalized Schiff bases and their metal complexes,[22] with tunable and switchable properties relevant to a wide variety of materials-related applications.[23] Fine-tuning and switching of the second-order nonlinear optical (NLO) responses of such appended ferrocene chromophores can be achieved owing to the stability of its accessible Fe(II)/Fe(III) redox states.[23-25]

Schiff bases, characterized by an imine (>C=N-) or an azomethine (-CH=N-) group ,[26,27] form an outstanding class of proligands that plays a key role in the development of coordination chemistry due to their facile synthesis, structural flexibility, easily tunable electronic properties, selectivity and sensitivity towards the coordinated metal ion and their ability to form stable complexes under various coordination geometries and oxidation states.[22,28-30] Transition-metal complexes of Schiff base ligands have been widely investigated because of their applications in various branches of science such as in catalysis,[31-33] sensing,[34-36] as NLO molecular materials,[23,37-39] and in biochemistry,[40-42] among others. Ferrocene substituted asymmetric N_2O_2-tetradentate Schiff bases are generally obtained upon condensation of salicylaldehyde or its derivatives with a preformed tridentate organometallic precursor bearing a free amino group.[22,39] These latter tridentate proligands featuring O,N,N-donor sets, so-called half-units,[43] result from a monocondensation of a ferrocenoyl-ketones of the type Fc-C(O)CH_2C(O)R (R = CH_3, 4-C_6H_4OH) with either 1,2-diaminoethane or 1,2-phenylenediamine.[44-46]

Interestingly, introduction of two asymmetric carbon atoms of a chiral diamine, such as 1,2-diphenylethylenediamine or 1,2-diaminocyclohexane, has been developed to force the crystallization of Schiff base complexes into a noncentrosymmetric space group, a prerequisite to observe second-harmonic generation.[37,47,48] Therefore, the development of a simple and

useful strategy for the preparation of chiral ferrocene substituted ONN-tridentate Schiff bases and their corresponding N_2O_2-tetradentate proligands and complexes is of noteworthy interest. In this prospect, we wish to report herein the synthesis, spectroscopic characterization and redox properties of (i) two ferrocene functionalized Schiff bases (**3** and **4**) derived from condensation of ferrocenoyl-acetone **1** and its 4-hydroxiphenyl substituted derivative **2** with enantiomerically pure (1R,2R)-(−)-1,2-diaminocyclohexane, respectively (see formulas in Scheme 1), and (ii) their related zinc(II) and palladium(II) complexes **5** and **6**, respectively, prepared via a metal-templated reaction in presence of the desired salicylaldehyde substrate (Scheme 2). The crystal structures of the chiral half-units **3** and **4** are also disclosed. The experimental data are complemented by DFT and TD-DFT calculations to elucidate aspects of the electronic structure and spectroscopic properties of the new complexes.

Results and discussion

Synthesis and characterization

The two tridentate Schiff-base proligands (1R,2R)-(−)-Fc-C(=O)CH=C(R)NH-*o*-C_6H_{10}-NH_2 (**3**: R= CH_3, **4**: R = 4-C_6H_4OH) were readily prepared by single condensation of the corresponding organometallic diketone Fc-C(=O)CH_2C(=O)R (**1**: R= CH_3, **2**: R = 4-C_6H_4OH), and a slight excess of enantiomerically pure (1R,2R)-(−)-1,2-diaminocyclohexane in refluxing ethanol for 4-5 h (Scheme 1). Half-units **3** and **4** were isolated in 81% and 72% yields, respectively, as red microcrystalline solids after flash chromatography purification on silica gel.

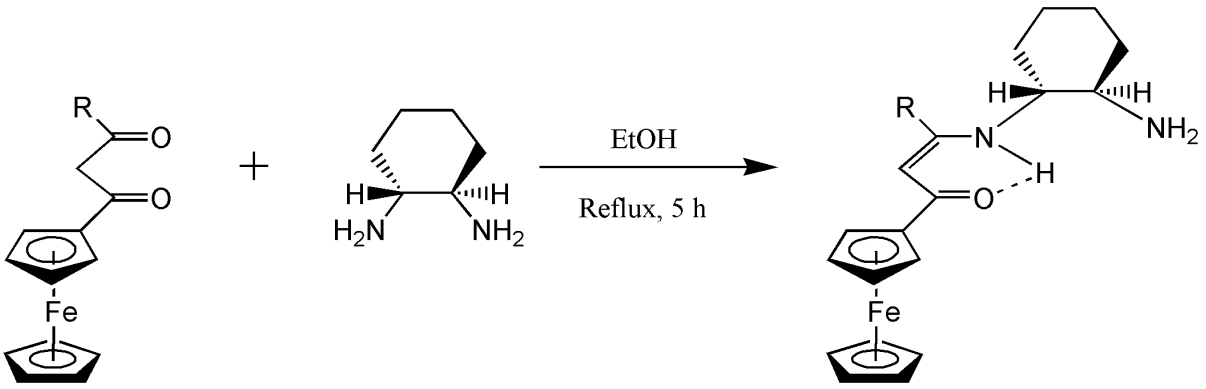

1: R = CH_3
2: R = 4-C_6H_4OH

3: R = CH_3
4: R = 4-C_6H_4OH

Scheme 1 Synthesis of the half-units **3** and **4**.

Bimetallic complexes **5** and **6** were prepared via an one-pot three-components template procedure involving the tridentate proligand **3**, 2-hydroxy-4-methoxybenzaldehyde and tetrahydrated zinc(II) nitrate for **5**, and half-unit **4**, 4-formyl-3-hydroxybenzoic acid and palladium(II) acetate for **6**, in a 1:1:1 ratio under reflux conditions (Scheme 2). Synthesis of the Zn(II) derivative **5** required harsher conditions (addition of NEt_3 and 24 h of reflux) than those used for preparing **6** (only 2h of reflux without base).

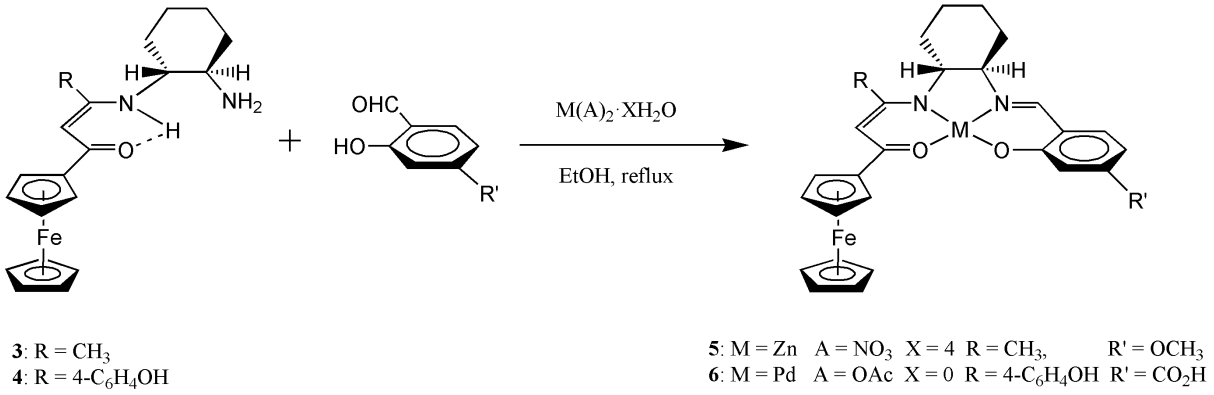

3: R = CH_3
4: R = 4-C_6H_4OH

5: M = Zn A = NO_3 X = 4 R = CH_3, R' = OCH_3
6: M = Pd A = OAc X = 0 R = 4-C_6H_4OH R' = CO_2H

Scheme 2 Synthesis of the bimetallic Zn(II) and Pd(II) complexes **5** and **6**.

The four new compounds **3-6** are all air and moisture compatible, thermally stable, exhibit a good solubility in common organic solvents, are poorly soluble in alcohols and insoluble in diethyl ether and hydrocarbons. Their composition, purity and formulation were established from satisfactory combustion analyses, FT-IR and UV-vis spectroscopy, multidimensional ^{1}H and ^{13}C NMR experiments, and single-crystal X-ray diffraction study (for **3** and **4**). In addition, electro spray ionization mass spectrometry (ESI-MS) confirmed the molecular composition of the four complexes with well detectable ion peaks at m/z (a.u.) = 389 $[M + Na]^+$, 427 $[M - OH]^{\cdot+}$ and 445 [M + H]+, 562 $[M]^{\cdot+}$, and 695 $[M - H]^{\cdot-}$, for **3-6**, respectively (see Experimental Section for details). For all these peaks, the envelope of the isotopic pattern was in good agreement with the simulated iones (Fig. S1-S4, ESI†).

The solid-state FT-IR spectra (KBr pellets) of the half-units **3** and **4** (Fig. S5 and S6, ESI†) exhibit both the asymmetric and symmetric stretching vibrations and the deformation mode of the terminal NH_2 group at 3369/3350, 3352/3279 and 1518/1471 cm^{-1}, respectively.[44-46] Both spectra show also a lower energy band at 3274 and 3207 cm^{-1} due to the stretching vibration of the enamine N-H group.[49] Although the complete disappearance of the bands between 3300 and

3400 cm^{-1} could not be confirmed in the spectra of **5** and **6**, due to the presence of the strong absorption of water molecules, the observation of the bands ν(C···N) at 1642 and 1607 cm^{-1}, and ν(C−O) at 1315 and 1280 cm^{-1} in the spectra of complexes **5** and **6** (Figs. S5 and S6, ESI†), respectively, strongly suggest the formation of the N_2O_2-tetradentate macroacyclic Schiff base ligand and its dianionic coordination mode to the central metal(II)- ion through the imine nitrogen and phenolato oxygen atoms.[50] The phenolic ν(O–H) band, appearing about 3430 cm^{-1}, is also observed in both the spectra of half-unit **4** and its related complex **6**. Moreover, in **6**, the carboxylic acid substituent is identified by the ν(C=O) vibration seen at 1680 cm^{-1}.[39]

The ^{1}H NMR spectra of the four compounds **3-6**, recorded in DMSO-d_6 at 298 K, displayed the expected resonance patterns consistent with the proposed structures (see Experimental Section for complete assignments and Fig. 1, and Fig. S7 and S8 ESI†). The singlets observed in the δ_H 3.99-4.13 ppm and δ_H 5.17-5.37 ppm ranges with integral ratio 5:1 are due to the free cyclopentadienyl ring and methine protons of the ferrocenyl enaminoketone fragment, respectively. In **3** and **5**, the methyl protons showed up as singlets at δ_H 2.03 and 2.11 ppm. In **4** and **6**, the 4-hydroxyphenyl substituent is characterized by two doublets in the δ_H 6.24-7.37 ppm range and a broad singlet about δ_H 9.85 ppm. Moreover, in the high field region, the aliphatic proton signals corresponding to the chiral (1R,2R)-cyclohexan-diyl unit are well-resolved and have all been assigned (see Experimental Section for details). The signals showing up at δ_H 8.20 and 7.99 ppm in the spectra of the bimetallic species **5** and **6** are attributed to the azomethine proton resonance, testifying the assembling of the N_2O_2 macrocyclic Schiff base framework. The salicylidene protons gave rise to three distinct resonances in the aromatic area and in the spectrum of **5** the methoxy substituent is observed at δ_H 3.68 ppm.

Both half-units **3** and **4** exist as their enaminone tautomeric form in solution.[49] Their respective ^{1}H NMR spectrum displays a deshielded amino proton signal at δ_H 10.90 and 10.67 ppm. This deshielding is due to intramolecular hydrogen bonding between the N-H group and the carbonyl oxygen atom. A similar result was also obtained for ferrocenyl-containing ONN-tridentate Schiff base when the 1,2-ethan-diyl spacer is used in place of the 1,2-cyclohexan-diyl one.[44,46] By contrast, formation of a 60/40 mixture of keto-enamine/keto-imine tautomers has been reported in the case of an *o*-phenylene spacer.[45]

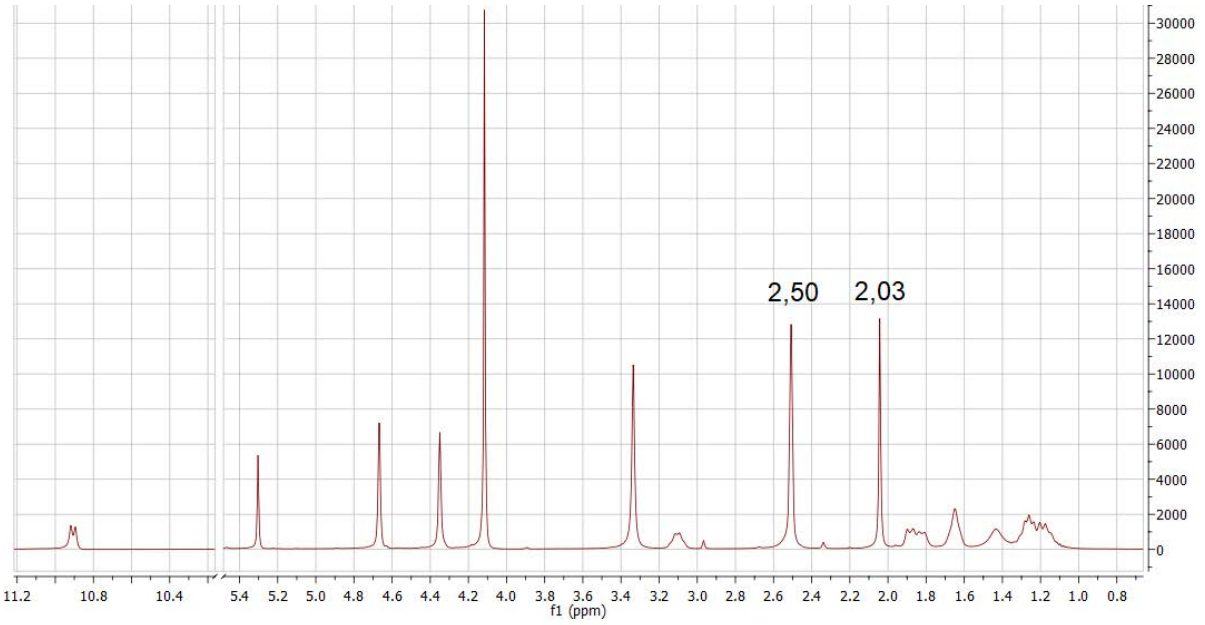

Fig. 1 ^{1}H NMR spectrum of half-unit **3** recorded in DMSO-d_6 at 298 K.

The $^{13}C\{^{1}H\}$ NMR spectra of **3-6** (Fig. 2 and Fig. S9-S11 ESI†) fully reproduce the features observed in ^{1}H NMR and support the interpretation outlined above, clearly demonstrating the asymmetric nature of the four compounds. Indeed, for each of them, each type of carbon gives rise to a specific signal except for **4** and **6** for which some resonances were not observed because of the poorer solubility of those complexes (see the Experimental Section for detailed assignment). As expected, the keto–enamine tautomeric form of half-unit **3** is confirmed with the methyne carbon resonance at 92.3 ppm.[44-46] On the other hand, the two resonances at 70.0 (C_α) and 67.8 (C_β) of the substituted cyclopentadienyl ring carbons (Chart 1) observed in the spectrum of complex **3**, are split into four signals at 70.0 (C_α), 69.9 ($C_{\alpha'}$), 67.9 (C_β) and 67.8 ($C_{\beta'}$) for the related bimetallic derivative **5** (Fig. 2). This splitting, not observed in the less resolved spectrum of the Pd(II) complex **6**, might result from a restricted rotation of the ferrocenyl unit about the C_{ipso}-$C_{carbonyl}$ bond, owing to the formation of the rigid $M(N_2O_2)$ Schiff base complex framework. One can also note that the chemical shift of the carbonyl carbon (~190 ppm) in the Schiff base proligands **3** and **4** remains unaffected upon oxygen coordination to the Zn(II) metal ion in **5**, while it is upfield shifted by about 16 ppm in **6**. Similar behaviors have previously been observed for Zn(II) and Pd(II) complexes of N_2O_2 tetradentate Schiff base ligands.[39,51,52]

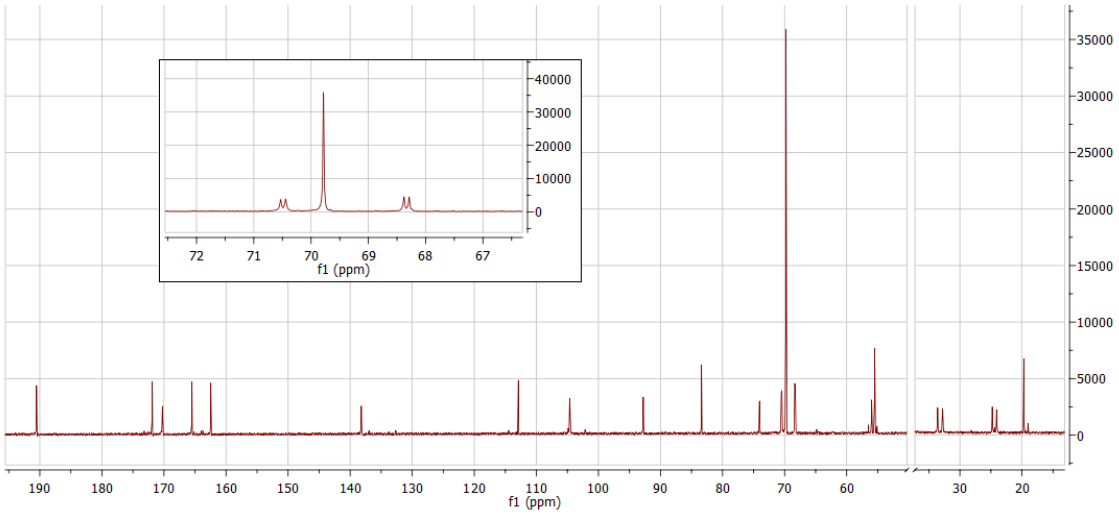

Fig. 2 $^{13}C\{^{1}H\}$ NMR spectrum of bimetallic complex **5** recorded in DMSO-d_6 at 298 K. Inser: resonance pattern of the substituted Cp carbons.

Crystal structural studies of the ferrocene-containing Schiff bases 3 and 4

Diffraction-quality single crystals for X-ray structure investigation were obtained for **3** and **4** using the slow diffusion crystallization method (see Experimental Section). The molecular structures of **3** and **4**, which crystallized as its isopropanol solvate **4**·^{i}PrOH, are displayed in Fig. 3, with selected bond distances and angles provided in Table 1. Both compounds crystallize in the orthorhombic non-centrosymmetric space group $P2_12_12_1$ with a single molecule in the asymmetric unit. The cyclohexan-diyl rings adopt a chair conformation, and the ferrocenyl moieties with parallel and eclipsed cyclopentadienyl rings features a typical linear η^5-Fe-η^5 sandwich structure.[5] Selected metrical parameters are summarised in Table S1 (ESI†).

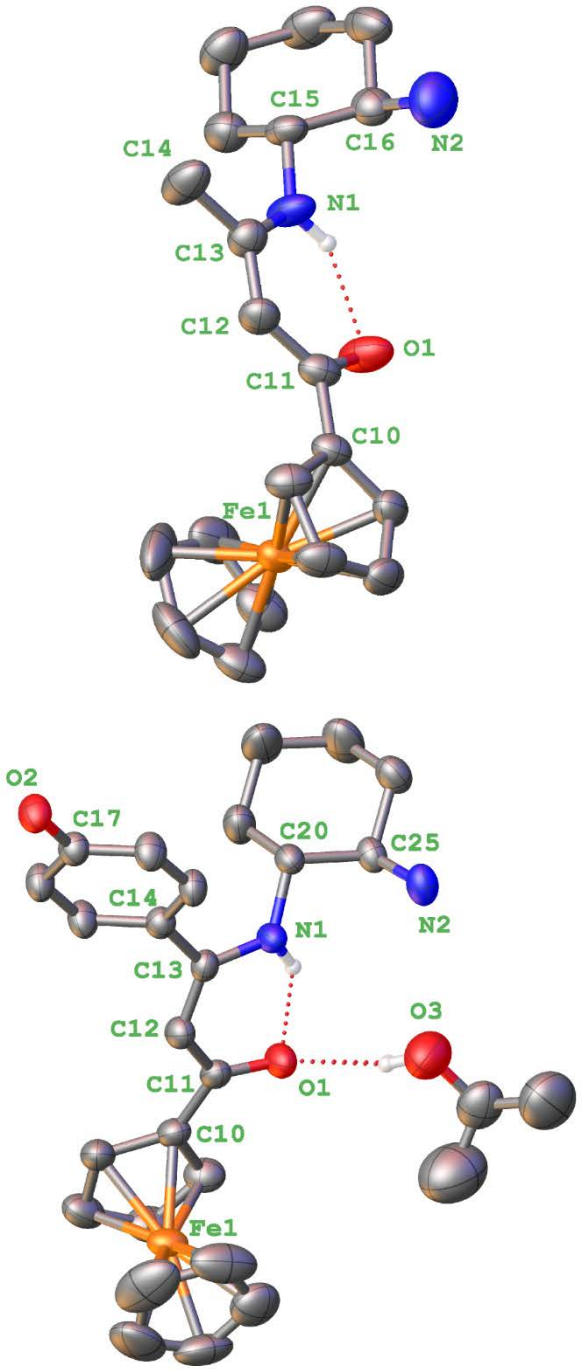

Fig. 3 Molecular structures of the ferrocene-containing chiral Schiff base proligands **3** (top) and **4**·iPrOH (bottom) with numbering scheme for selected atoms. Hydrogens, except those involved in the N(1)-H···O(1) hydrogen bonding interaction, are omitted for clarity. Thermal ellipsoids are drawn at 50 % probability.

Table 1 Selected experimental (X-ray) bond distances (Å) and angles (°) for compounds **3** and **4**·^{i}PrOH. The corresponding DFT-optimized values are given into brackets.

3			**4**·^{i}PrOH	
Bond distances				
O(1)-C(11)	1.248(4) [1.245]		O(1)-C(11)	1.249(4) [1.239]
C(10)-C(11)	1.496(5) [1.478]		C(10)-C(11)	1.479(4) [1.478]
C(11)-C(12)	1.412(5) [1.429]		C(11)-C(12)	1.421(4) [1.437]
C(12)-C(13)	1.381(5) [1.376]		C(12)-C(13)	1.377(4) [1.371]
C(13)-C(14)	1.500(5) [1.496]		C(13)-C(14)	1.481(4) [1.473]
N(1)-C(13)	1.321(5) [1.336]		N(1)-C(13)	1.360(4) [1.352]
N(1)-C(15)	1.468(4) [1.442]		N(1)-C(20)	1.467(4) [1.454]
N(2)-C(16)	1.458(6) [1.450]		N(2)-C(25)	1.473(5) [1.452]
C(15)-C(16)	1.526(5) [1.537]		C(20)-C(25)	1.533(4) [1.527]
			O(2)-C(17)	1.354(4) [1.355]
Fe-C_{Cp} av.	2.029(4) [2.032]		Fe-C_{Cp} av.	2.034(5) [2.034]
Fe-$C_{Cp'}$ av.	2.036(4) [2.032]		Fe-$C_{Cp'}$ av.	2.041(4) [2.033]
Bond angles				
O(1)-C(11)-C(12)	123.70(3) [123.3]		O(1)-C(11)-C(12)	123.3(3) [123.5]
N(1)-C(13)-C(12)	121.10(3) [121.0]		N(1)-C(13)-C(12)	120.8(3) [121.8]
C(11)-C(12)-C(13)	123.80(3) [122.9]		C(11)-C(12)-C(13)	124.0(3) [123.2]
C(13)-N(1)-C(15)	128.50(3) [127.3]		C(13)-N(1)-C(20)	125.8(2) [123.3]
N(1)-C(15)-C(16)	108.50(3) [109.5]		N(1)-C(20)-C(25)	107.1(2) [109.7]
N(2)-C(16)-C(15)	115.20(3) [114.8]		N(2)-C(25)-C(20)	113.0(3) [114.7]

Cp = η^5-C_5H_5, Cp' = η^5-C_5H_4.

The molecular structures show that both compounds adopt the Z-*s*-Z conformation,[49] consistent with a keto-enamine tautomeric isomer.

An intramolecular N(1)-H···O(1) hydrogen bond with $d_{N\cdots O}$ = 2.657(4) Å and 2.675(3) Å (Table S2, ESI†) closes the planar pseudo six-membered ring through a resonant

⋯O(1)=C(11)-C(12)=C(13)-N(1)-H fragment,[53] with alternating double-, single-, double- and single-bonds between the vicinal sp^2-hybridized atoms (Table 1).[54] In **3**, the plane of the enaminone core is coplanar with that of the substituted cyclopentadienyl ring, making a dihedral angle of 3.7(2)°, and twisted by 15.6(2)° in **4**·^{i}PrOH. In this latter, it also makes a torsion angle of 39.3(1)° with the plane of the phenol ring. All those metrical parameters are in accordance with previously reported structural data for related ferrocene-containing enaminone derivatives.[44-46,55]

Finally, in **4**·^{i}PrOH the crystal packing is stabilized by intermolecular hydrogen bonds between the hydroxy O(2)-H group and the nitrogen N(2) of the free amino group of neighboring molecules ($O(2)\cdots N(2)^{\#1}$ = 2.692(4) Å, #1: x, y, z) to give a zig-zag chain, a ladder-type arrangement, oriented along the y-axis (Fig. S12, ESI†). In addition, the disordered isopropanol crystallization molecule found in the asymetric unit interacts also with the N(2) atom and the carbonyl oxygen (O(1)) of half-unit **4** through intermolecular hydrogen bonds, with N⋯O and O⋯O separations of 3.205(5) Å and 2.841(4) Å, respectively (Table S2, ESI†).

Electronic absorption spectroscopy

The UV-vis absorption spectra of the four compounds **3-6** were recorded in the 250-800 nm range in both dichloromethane (DCM) and dimethylformamide (DMF) solutions at room temperature. The experimental spectra are presented in Fig. 4. They are mainly composed of a broad absorption band which, upon deconvolution with Gaussian curves, give rise to two, or four in the case of **6**, transitions (Table 2). The higher energy bands (315-368 nm) are based on π-π* transitions due to the imine groups and aromatic rings, and are associated with intra-ligand charge transfers (ILCT). For compounds **3-5**, the bands of lower energy (461, 470 and 546 nm, respectively) are mainly influenced by M→π* metal-to-ligand charge transfers (MLCT) transitions, while that seen at 461 nm for **6** is assigned to a ligand-to-ligand charge transfer (LLCT) transition (see below Theoretical section). All those major features of the experimental spectra are reproduced on passing from DCM to the more polar DMF solvent. The bands exhibit either bathochromic or hypsochromic shifts (Table 2), characteristic of a dipole moment change between the ground and excited state, and indicative of a CT character. Such a solvatochromism is also characteristic of push-pull complexes and could be related to potential NLO properties.[39,51,56]

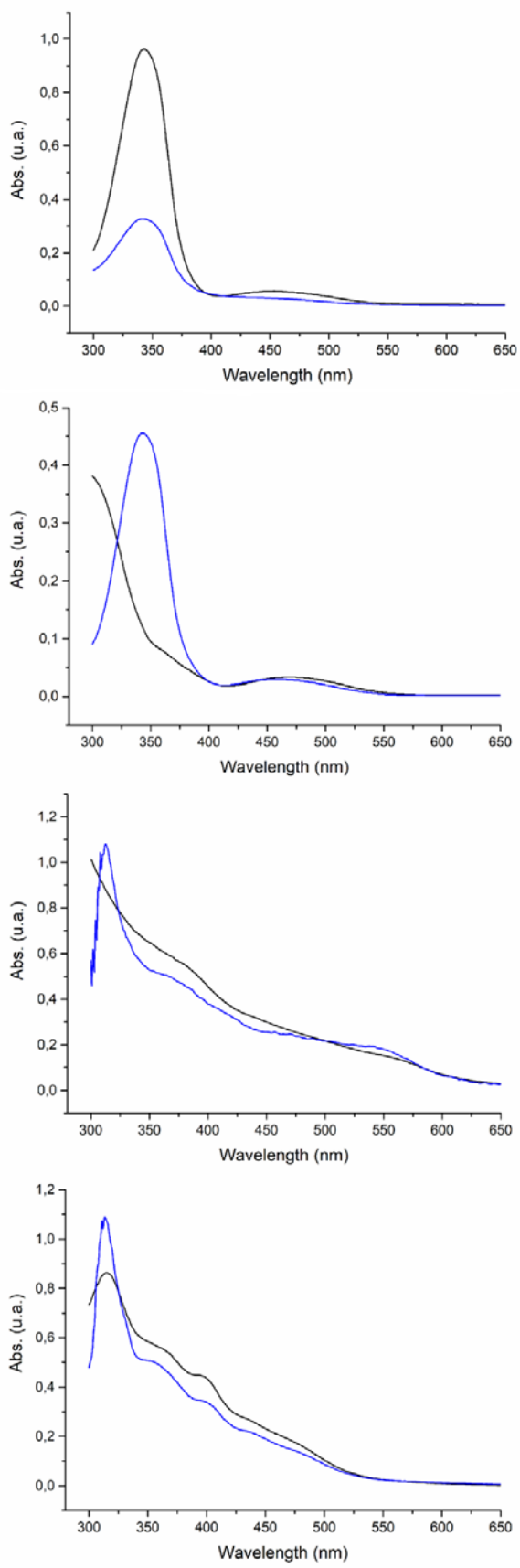

Fig. 4 UV-vis spectra of the ferrocene-containing Schiff base compounds **3-6** (from top to bottom) recorded in dichloromethane (black line) and DMF (blue line). Solutions at 20 °C.

Table 2 UV-vis absorption data for compounds **3-6**. The last column lists the λ_{max} values from the TD-DFT-simulated spectra.

Compd.	λ / nm (Log ε) (DCM)	λ / nm (Log ε) (DMF)	Solv. shift / cm^{-1}	λ / nm (TD-DFT)
3	341 (4.69) 461 (3.46)	339 (4.20) 442 (3.21)	-173 -932	360 483
4	358 (3.61) 470 (3.24)	343 (4.36) 457 (3.14)	-1222 -605	311 485
5	370 (4.43) 546 (4.05)	383 (4.44) 561 (3.84)	+917 +490	307 495
6	315 (4.58) 368 (4.34) 397 (4.24) 461 (3.73)	314 (4.69) 355 (4.30) 400 (4.08) 460 (3.55)	-101 -995 +189 -47	293 331 433

Electrochemical study

The electrochemical behaviour of the two half-units **3** and **4**, and of their respective bimetallic Schiff base derivatives **5** and **6** was investigated using cyclic voltammetry (CV) in DMF containing 0.1 M [*n*-Bu_4N][PF_6] as supporting electrolyte. The CV measurements were carried out at room temperature in the 0.0 to 1.0 V vs. Ag/AgCl potential range with scan rate of 100 $mV \cdot s^{-1}$ (Fig. 5, Fig. S13, ESI†). Each of the four compounds displays one chemically reversible redox process due to the monoelectronic oxidation of the ferrocenyl moiety,[57] with current ratio i_{pa}/i_{pc} equal to unity. The redox potentials of the four compounds are anodically shifted by 70-270 mV with respect to free ferrocene under the same electrochemical conditions (Table 3), clearly illustrating the electron withdrawing effect of the Schiff base side chain substituent. The $E_{1/2}$ values measured for the two half-units **3** and **4** are almost identical and in accordance with those previously reported for their counterparts formed from 1,2-diaminoethane and 1,2-diaminobenzene.[44,45] The electrochemical behavior of the two bimetallic derivatives **5** and **6** confirms a trend already observed.[39,51,52] That is a weak anodic shift in the case of Zn(II) and a large one in the case of Pd(II) complexes, whatever the substituent borne by the salicylidene ring. In the Zn(II) series, the same 70 mV anodic shift was found for both **5** substituted by the methoxy donor group and its previously reported relative bearing the electron withdrawing nitro group.[51] This anodic behaviour could result from the coordination environment at the metal center. From the DFT-optimized geometry (see below and Table 4), the Zn(II) metal ion adopts a tetrahedrally distorted coordination sphere (τ_4 =

0.435),[58] thus almost switching the conjugation between the end groups of the molecules. On the other hand, the large anodic shift value of 270 mV determined for Pd(II) complex **6** (Table 3), corroborates our previous data (180-240 mV) obtained with related Pd(II) complexes featuring ferrocenyl-containing N_2O_2 tetradentate Schiff base ligands.[39,52] In the case of compound **6**, the Pd(II) metal ion lies in a quasi-perfect square-planar environment (τ_4 = 0.057),[58] thus greatly facilitating the electronic communication between the ferrocenyl donor and the $–CO_2H$ acceptor parts of the molecule.

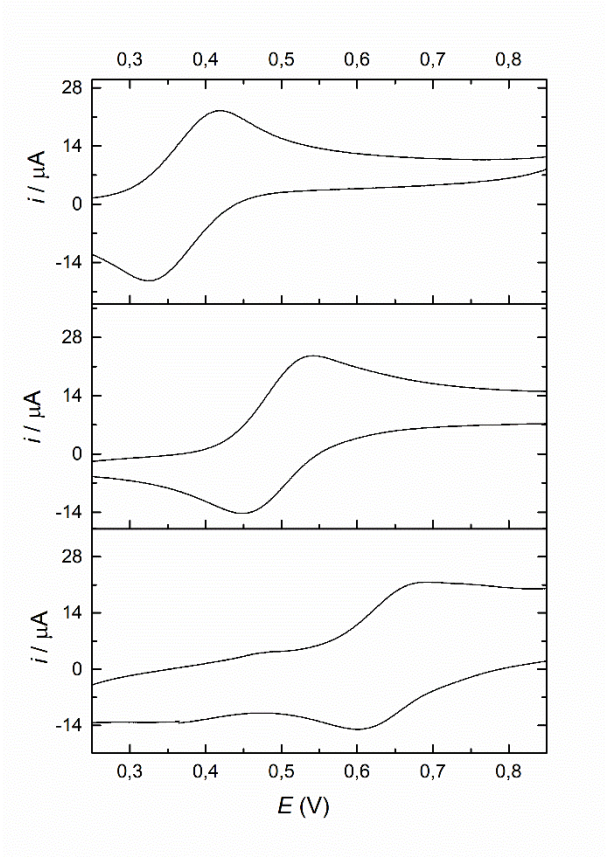

Fig. 5 Cyclic voltammograms of free ferrocene (top), half-unit **4** (middle) and of the bimetallic complex **6** (bottom) recorded at a vitreous carbon working electrode in DMF containing 0.1 M [*n*-Bu_4N][PF_6], T = 298 K, v = 100 mV s^{-1}; reference electrode Ag/AgCl.

Table 3 Formal electrode potentials and peak-to-peak separations for the Fe^{II}/Fe^{III} redox processes exhibited by compounds **3-6**.[a]

Compd.	$E_{1/2}$/V	ΔE_p/mV
3	0.47	118
4	0.49	93
5	0.44	64
6	0.64	79
Cp_2Fe	0.37	97

[a] Recorded at a vitreous carbon working electrode in DMF containing 0.1 M [*n*-Bu_4N][PF_6] at T = 298 K with a sweep rate v = 100 mV s^{-1}, reference electrode Ag/AgCl.

Theoretical investigations

Density functional theory (DFT) calculations at the PBE0/TZ2P level were performed to optimize the geometries of complexes **3-6** (see Computational Details). The four optimized structures are shown in Fig. 6. Selected computed data are provided in Tables 1 and 4. The optimized geometries of **3** and **4** are in good agreement with their X-ray structures (compare Fig. 3 and 6 and the values in the Table 1). The hydrogen bonding between the N-H group and the carbonyl oxygen atom in **3** and **4** (N(1)-H···O(1)) is confirmed by DFT, with H···O(1) distances of 1.763 and 1.800 Å, respectively. The associated N(1)-H stretching vibration frequency computed for **3** (3280 cm^{-1}) is in very good agreement with its experimental counterpart (3274 cm^{-1}). The agreement is not as good in the case of **4** (3320 *vs.* 3207 cm^{-1}), perhaps due to interactions with solvent molecules (as in the X-ray structure), not considered in the calculation.

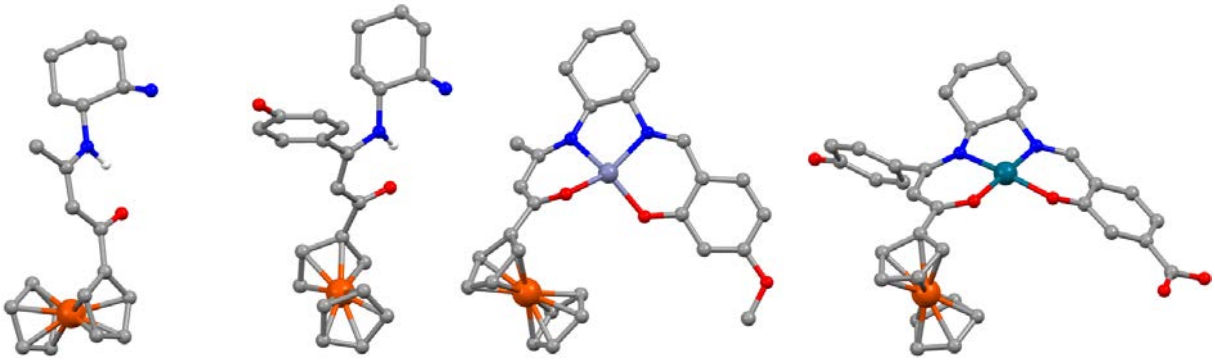

3 **4** **5** **6**

Fig. 6 DFT-optimized geometries of complexes **3-6**. Hydrogens, except those involved in the N(1)-H···O(1) hydrogen bonding interaction in **3** and **4**, are omitted for clarity.

Unsurprisingly, the ferrocenyl units of the four complexes have similar geometrical features. As expected for a d^8 metal center, the Pd(II) metal in **6** lies in an approximate square-planar environment (sum of bond angles at Pd = 359.9°). The d^{10} Zn(II) center in **5** affords a significant tetrahedral distortion, as exemplified by the far from 180° values of the *trans* N-Zn-O angles in Table 4 and by the sum of bond angles at Zn (373.1°).

Table 4 Selected optimized bond distances (Å) and angles (°) for compounds **5** and **6**.

5			**6**	
Zn-N_{amin}	2.020		Pd-N_{amin}	1.981
Zn-N_{imin}	1.994		Pd-N_{imin}	1.950
Zn-O_{phen}	1.923		Pd-O_{phen}	1.995
Zn-O_{carb}	1.929		Pd-O_{carb}	1.980
Fe-C_{Cp} av.	2.033		Fe-C_{Cp} av.	2.034
Fe-$C_{Cp'}$ av.	2.035		Fe-$C_{Cp'}$ av.	2.033
N_{am}-Zn-O_{phen}	143.0		N_{am}-Pd-O_{phen}	172.5
N_{imin}-Zn-O_{carb}	155.6		N_{imin}-Pd-O_{carb}	179.4

Abbreviations: Cp = η^5-C_5H_5; Cp' = η^5-C_5H_4; amin = amino; imim = imino; phen = phenolato; carb = carbonyl.

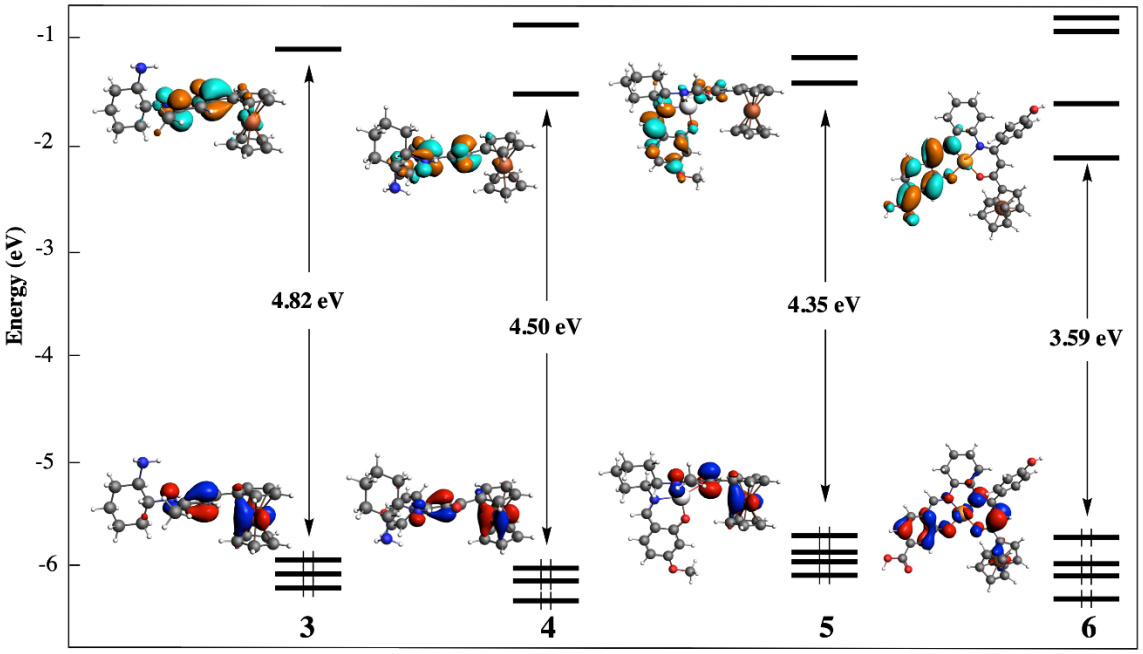

Fig. 7 The Kohn-Sham orbital diagrams of **3**-**6**.

The Kohn-Sham orbital diagrams of **3-6** are shown in Fig. 7. They exhibit rather similar features. In the case of complexes **3-5**, the HOMO is major, but not exclusive, 3d(Fe) character (54%, 61% and 51% for **3**, **4** and **5** respectively), with lower, but significant, ligand character (Fig. 7). This orbital is the highest member of the three MOs associated with the six Fe(II) 3d electrons (the so-called ferrocenyl "t_{2g} set"). In the case of **6**, these three levels are situated below the HOMO, which is of dominant ligand character with some minor participation of Pd (11%) and Fe (9%). In the four complexes, the LUMO is of π*-ligand character. In the case of **3** and **4**, it is localized on the unique conjugated part of the ligand, whereas in the case of **5** and **6**, it is centered on the N=C bond and the attached C_6 ring. In compounds **5** and **6**, the M-centered levels (M = Zn, Pd) lie significantly below the HOMO and thus are not involved in the oxidation process. The computed ionization energies (IE, see computational details) for complexes **3-6** and ferrocene are 6.76, 6.76, 6.50, 5.93 and 7.06 eV, respectively. The variation of these values do not match with that of the corresponding electrode potentials listed in Table 3. The discrepancy is likely at least in part due to the non-explicit consideration of the coordinating DMF solvent in the calculations. In the four complexes, the oxydation occurs at the Fe center, including the case of **6**, as shown by the plots of the spin density of the $\mathbf{3}^{+}$-$\mathbf{6}^{+}$ cations (Fig. 8) which is largely localized on Fe (1.3 a.u. for the four complexes, as compared to 0.7 in ferrocenium).

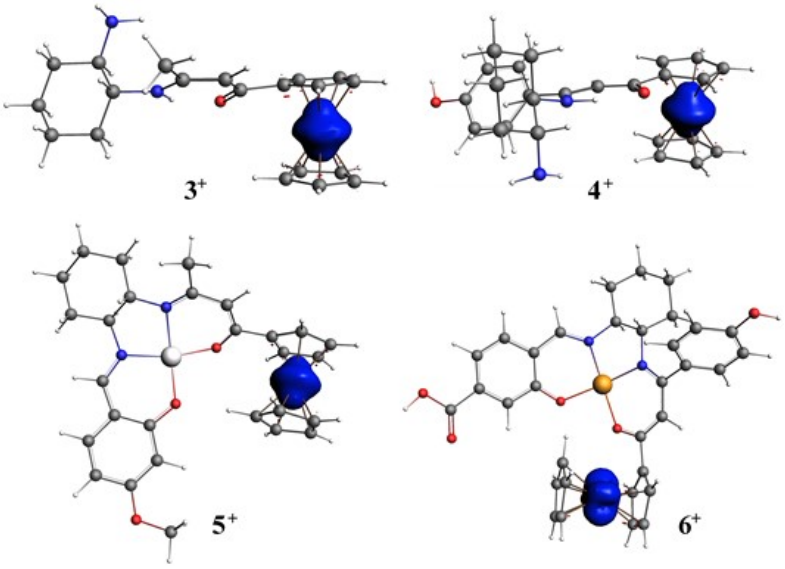

Fig. 8 Plots of the spin densities of the **3**$^{+}$-**6**$^{+}$ cations (surface isovalue: 0.005 a.u.).

Time-dependent density functional theory (TD-DFT) calculations were subsequently performed at the PBE0/TZ2P level on the optimized geometries to simulate the UV-vis spectra of **3-6**. The simulated spectra are shown in Fig. S14 (ESI†) and their maximum absorption values are provided in Table 2. The agreement with the experimental spectra is satisfying, particularly on its low-energy part. In the four compounds, the weak band of lowest energy is associated with FeLCT character, except for **6** where it is associated with the HOMO→LUMO transition (LLCT). The next absorption band is of FeLCT nature for the four compounds.

Conclusions

To summarize, we have isolated and fully characterized a series of four ferrocene functionalized enantiomerically pure N_2O-tridentate and N_2O_2-quadridentate Schiff base complexes, using the enantiomericaly pure (1R,2R)-(−)-1,2-diaminocyclohexane as the chiral source. The two ferrocenyl enaminones were readily synthesized by a straightforward 1:1 condensation of ferrocenoylacetone and (1R,2R)-(−)-1,2-diaminocyclohexane, while the two bimetallic species were prepared via a three-component one-pot template reaction involving the appropriate ferrocenyl-containing half-unit, metal(II) salt and salicylaldehyde derivative. Single crystal X-ray diffraction study of the two half-units showed that the two compounds crystallize in the orthorhombic non-centrosymmetric space group $P2_12_12_1$ with two (R,R)-(−)-chiral carbon atoms in their structure, and that they exist only as their keto-enamine tautomeric

form in the solid state. The electrochemical analysis nicely illustrates through the strong anodic shift of the ferrocene/ferrocenium redox couple that the electronic communication between the electron releasing and withdrawing groups is particularly facilitated in the case of the bimetallic species having the d^8 square-planar Pd^{II} as the central metal ion. DFT calculations enable assessing the structure of **5** and **6** and to shed some light on the electronic structure of the four complexes, confirming that Fe(II) is the oxidation center in the four complexes. TD-DFT calculations allows to assign the UV-vis transitions as of FeLCT character, except in the case of **6** where the band of lowest energy is of major LLCT nature. Furthermore, for elaboration of functionalized materials, –OH and $–CO_2H$ linkers are attractive sites for anchoring the complexes onto various supports.

Experimental Section

Materials and physical techniques

All manipulations were carried out under a dinitrogen atmosphere using standard Schlenk techniques. The solvents were dried and distilled according to standard procedures.[59] Pure enantiomerically (1R,2R)-(−)-1,2-diaminocyclohexane, 4-formyl-3-hydroxybenzoic acid, 2-hydroxy-4-methoxybenzaldehyde (*m*-vanillin), palladium(II) acetate and zinc(II) nitrate tetrahydrate were purchased from Aldrich and used without further purification. The 1-ferrocenyl-1,3-butanedione (**1**)[60] and the 1-ferrocenyl-3(4-hydroxyphenyl)-1,3-propanedione (**2**)[46] were synthesized according to literature procedures. Solid-state FT-IR spectra were recorded on a Perkin-Elmer Model 1600 FT-IR spectrophotometer with KBr disks in the 4000 to 450 cm^{-1} range. Electronic spectra were obtained with a SHIMADZU UV-1800 spectrophotometer. ^1H and $^{13}C\{^1H\}$ NMR spectra were obtained at 298 K on a Bruker Avance III 400 or Avance 500 spectrometer. All NMR spectra are reported in parts per million (δ, ppm, δ) relative to tetramethylsilane (Me_4Si), with the residual solvent proton and carbon resonances used as internal standards. Coupling constants (*J*) are reported in Hertz (Hz), and integrations are reported as number of protons. The following abbreviations are used to describe peak patterns: s = singlet, d = doublet, t = triplet, m = multiplet, br = broad. ^1H and ^{13}C NMR chemical shift assignments are supported by data obtained from ^1H-^1H COSY, ^1H-^{13}C HMQC, and ^1H-^{13}C HMBC NMR experiments, and are given according to the numbering scheme depicted in Chart 1. High resolution electrospray ionization mass spectra (ESI-MS) were obtained at the Centre Regional de Mesures Physiques de l'Ouest (CRMPO, Université de Rennes1, France)

with WATERS Q-TOF 2 and Bruker MAXI 4G spectrometers. Elemental analyses were conducted on a Thermo-Finnigan Flash EA 1112 CHNS/O analyzer by the Microanalytical Service of the CRMPO. Cyclic voltammetry (CV) measurements were performed using a CH Instruments model Ch604E potentiostat (Ch Instruments Inc., Austin, TX, USA), using a standard three-electrode setup with a vitreous carbon working electrode, platinum wire auxiliary electrode, and Ag/AgCl as the reference electrode. Dimethylformamide (DMF) solutions were 2.0 mM in the compound under study and 0.1 M *n*-$Bu_4N^+PF_6^-$ as supporting electrolyte, with voltage scan rate = 100 mV s^{-1}. $E_{1/2}$ is defined as equal to $(E_{pa} + E_{pc})/2$, where E_{pa} and E_{pc} are the anodic and cathodic peak potentials, respectively. The ferrocene/ferrocenium redox couple (Cp_2Fe/Cp_2Fe^+) was used as internal reference for the potential measurements.

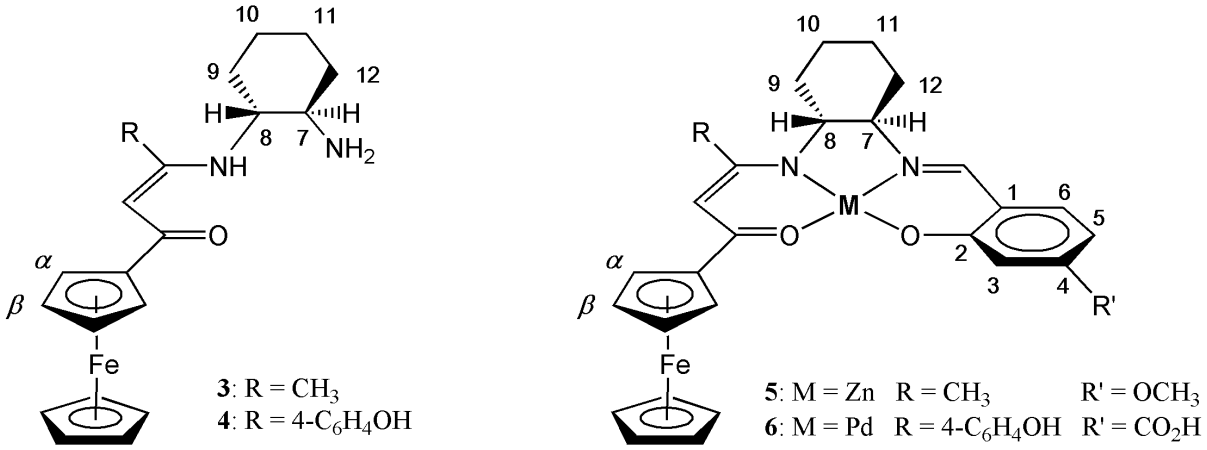

Chart 1 Labelling scheme used for NMR assignments.

Synthesis of (1R,2R)-(−)-Fc-C(=O)CH=C(CH_3)N(H)-*o*-C_6H_{10}-NH_2 (3)

To a stirred solution of 1-ferrocenyl-1,3-butanedione **1** (500 mg, 1.85 mmol) in ethanol (20 mL) in a Schlenk flask equipped with a condenser was added a solution of (1R,2R)-(−)-1,2-diaminocyclohexane (320 mg, 2.78 mmol) in ethanol (5 mL). The reaction mixture was refluxed for 5 h and, subsequently, evaporated to obtain a red oil that was absorbed on silica gel (70-230 mesh) and eluted with a diethyl ether/ethanol (9:1) mixture. The evaporation of the collected solution gave a red powder. Yield: 550 mg, 81%. X-ray quality orange crystals were obtained by slow diffusion of diethyl ether into a concentrated solution of **3** in ethanol. Elemental analysis (%) Calculated for $C_{20}H_{26}FeN_2O$ (366.29 g mol^{-1}): C, 65.58; H, 7.15; N, 7.65. Found: C, 65.42; H, 7.05; N, 7.52. ESI MS (*m*/*z*) calcd for $C_{20}H_{26}N_2ONa^{56}Fe$: 389.12922, found:

389.1289 $[M+Na]^+$. FT-IR (KBr, cm^{-1}): 3369(w) $\nu_{asym}(NH_2)$; 3352(w) $\nu_{sym}(NH_2)$; 3274(m) ν(N−H); 3097(m), 3085(w) ν(C−H arom); 2932(s), 2860(m), 2848(m) ν(C−H aliph); 1597(vs) ν(C⋯O); 1542(vs) ν(C⋯C); 1518(s) $\delta(NH_2)$; 725(s) δ(C−H). ^{1}H NMR (400 MHz, DMSO-d_6): 10.90 (d, 1 H, NH), 5.30 (s, 1 H, CH=C), 4.66 (s, 2 H, H_α C_5H_4), 4.34 (s, 2 H, H_β C_5H_4), 4.11 (s, 5 H, C_5H_5), 3.11 (m, 1 H, H-7), 2.50 (br s, 3 H, H-8 + H_2O/DMSO), 2.03 (s, 3 H, CH_3), 1.88 (m, 1 H, H-9b), 1.81 (m, 1 H, H-12b), 1.63 (m, 2 H, H-10b and H-11b), 1.25 (m, 2 H, H-10a and H-11a), 1.18 (m, 2 H, H9a and H12a); NH_2 protons not observed. ^{13}C{^{1}H} NMR (101 MHz, DMSO-d_6): 189.7 (C=O), 162.2 (CH=*C*), 92.3 (*C*H=C), 83.2 (C_{ipso} C_5H_4), 70.0 (C_β C_5H_4), 69.3 (C_5H_5), 67.8 (C_α C_5H_4), 59.2 (C-7), 55.3 (C-8), 34.0 (C-12), 32.7 (C-9), 24.5 (C-11), 24.1 (C-10), 19.3 (CH_3).

Synthesis of (1R,2R)-(−)-Fc-C(=O)CH=C(4-C_6H_4OH)N(H)-*o*-C_6H_{10}-NH_2 (4)

To a solution of Fc-C(=O)CH_2C(4-C_6H_4OH)=O (**2**) (0.50 g, 1.44 mmol) in ethanol (15 mL) in a Schlenk flask equipped with a condenser was added two drops of glacial acetic acid and slowly a solution of (1R,2R)-(−)-1,2-diaminocyclohexane (0.335 g, 2.88 mmol) in ethanol (5 mL). The reaction mixture was refluxed for 4 h and, subsequently, evaporated to obtain a red oil that was absorbed on silica gel (70-230 mesh) and eluted with a diethyl ether/ethanol (9:1) mixture. The evaporation of the collected solution gave a red powder of **4**, which was washed with cold methanol and diethyl ether (2 × 5 mL) and dried under vacuum. X-ray quality crystals were obtained by slow diffusion of diethyl ether into a solution of half-unit **4** in dimethylformamide (DMF)/isopropanol (1:1). Yield: 460 mg, 72,1 %. Elemental analysis (%) Calculated for $C_{25}H_{28}O_2N_2Fe$ (444.36 g mol^{-1}): C, 67.58; H, 6.35; N, 6.30. Found: C, 66.78; H, 6.39; N, 5.82. ESI MS (*m*/*z*) calcd for $C_{25}H_{27}N_2O^{56}Fe$: 427.14728, found: 427.1455 $[M. - OH]^+$; (*m*/*z*) calcd for $C_{25}H_{29}N_2O_2{}^{56}Fe$: 445.15784, found: 445.1579 $[M + H]^+$. FT-IR (KBr, cm^{-1}): 3432(w) ν(O-H); 3350(m) $\nu_{asym}(NH_2)$; 3279(m) $\nu_{sym}(NH_2)$; 3207(W) ν(N−H); 3106(m), 3094(m), 3085(m) ν(C−H arom); 2933(s), 2900(m), 2859(m) ν(C−H aliph); 1602(vs) ν(C⋯O); 1576(vs) ν(C⋯C); 1471(vs) $\delta(NH_2)$; 737(m) δ(C−H). ^{1}H NMR (400 MHz, DMSO-d_6): 10.67 (s, 1 H, NH), 9.80 (br s, 1 H, O-H), 7.37 (d, $^3J_{H,H}$ = 8.0 Hz, 2 H, C_6H_4), 6.86 (d, $^3J_{H,H}$ = 8.0 Hz, 2 H, C_6H_4), 5.37 (s, 1 H, <u>CH</u>=C), 4.73 (s, 2 H, H_α C_5H_4), 4.39 (s, 2 H, H_β C_5H_4), 4.13 (s, 5 H, C_5H_5), 3.32 (br s, 2 H, NH_2), 3.16 (s, 1 H, H-8), 2.94 (s, 1 H, H-7), 1.79 (m, 2 H, H-9b and H-12b), 1.56 (m, 2 H, H-11b and H-12a), 1.21 (m, 2 H, H-10b and H-11a), 1.04 (m, 2 H, H-9a

and H-10a). $^{13}C\{^{1}H\}$ NMR (100 MHz, DMSO-d_6): 190.7 (C=O), 132.9 (CH C_6H_4), 131.7 (CH C_6H_4), 70.1 (C_β C_5H_4), 69.1 (C_5H_5), 67.8 (C_α C_5H_4).

Synthesis of (1R,2R)-(−)-[Zn{Fc-C(=O)CH=C(CH_3)N-*o*-C_6H_{10}-N=CH-(2-O,4-OCH_3-C_6H_3)}] (5)

To a Schlenk tube containing a stirred solution of **3** (150 mg, 0.41 mmol) in ethanol (10 mL) was added dropwise 2-hydroxy-4-methoxybenzaldehyde (64 mg, 0.41 mmol) in ethanol (5 mL) and the solution was refluxed for 1 h. Subsequently, 1 mL of triethylamine was added, and the reflux was continued for 15 minutes. Then, a solution of zinc nitrate tetrahydrate (107 mg, 0.41 mmol) dissolved in 5 mL of ethanol was added and the reaction medium refluxed for 24 h. The orange powder of complex **5** was obtained by slow diffusion of diethyl ether into the reaction medium at -3°C for 48 h. The solid obtained was filtered, washed with cold methanol and diethyl ether (2 × 3 mL), and dried under vacuum. Yield: 163 mg, 71 %. Elemental analysis (%) Calculated for $C_{28}H_{30}FeN_2O_3Zn$ (563.78 g mol^{-1}): C, 59.65; H, 5.36; N, 4.97. Found: C, 61.20; H, 5.81; N, 5.00. ESI MS (*m*/*z*) calcd for $C_{28}H_{30}N_2O_3{}^{56}Fe^{64}Zn$: 562.08918, found: 562.0897 $[M]^+$. FT-IR (KBr, cm^{-1}): 3424(w) ν(OH), 3083(m), 3062(w) *ν*(C−H arom); 2930(s), 2854(m) *ν*(C−H aliph); 1642(vs) *ν*(C⋯N); 1558(s), 1545(s) *ν*(C⋯O) and/or ν(C⋯C); 1315(s) *ν*(C−O); 731(vw)*δ*(C−H). ^1H NMR (400 MHz, DMSO-d_6): 8.20 (s, 1 H, N=CH), 7.08 (d, $^3J_{H,H}$ = 8.3 Hz, 1 H, H-6), 6.15 (br s, 1 H, H-3), 6.13 (dd, 1 H, H-5), 5.17 (s, 1 H, CH=C), 4.61 (s, 2 H, H_α C_5H_4), 4.32 (s, 2 H, H_β C_5H_4), 3.99 (s, 5 H, C_5H_5), 3.69 (s, 3 H, OCH_3), 3.68 (m, 1 H, H-7), 3.21 (m, 1 H, H-8), 2.11 (s, 3 H, CH_3), 1.95 (m, 1 H, H-12b), 1.87 (m, 1 H, H-9b), 1.58 (m, 1 H, H-10b), 1.46 (m, 1 H, H-11b), 1.23 (m 1 H, H-12a), 1.19 (m, 1 H, H-11a), 1.15 (m, 1 H, H-9a), 0.77 (m, 1 H, H-10a). $^{13}C\{^{1}H\}$ NMR (100 MHz, DMSO-d_6): 190.0 (C=O), 171.4 (C-4), 169.5 (N=CH), 165.0 (C-2), 162.0 (CH=*C*), 137.7 (C-6), 104.1(C-3), 104.0 (C-5), 112.4 (C-1), 92.3 (*C*H=C), 82.9 (C_{ipso} C_5H_4), 73.5 (C-8), 70.0 (C_α C_5H_4), 69.9 ($C_{\alpha'}$ C_5H_4), 69.3 (C_5H_5), 67.9 (C_β C_5H_4), 67.8 ($C_{\beta'}$ C_5H_4), 55.5 (C-7), 55.0 (OCH_3), 33.1 (C-12), 32.13 (C-9), 24.3 (C-11), 23.6 (C-10), 19.2 (CH_3).

Synthesis of (1R,2R)-(−)-[Pd{Fc-C(=O)CH=C(4-C_6H_4OH)N-*o*-C_6H_{10}-N=CH-(2-O,4-CO_2H-C_6H_3)}] (6)

To a Schlenk tube containing a stirred solution of **4** (300 mg, 0.82 mmol) in ethanol (15 mL) was added dropwise 4-formyl-3-hydroxybenzoic acid (140 mg, 0.82 mmol) in ethanol (10 mL) and the stirring was continued for 5 min. Then, a solution of palladium(II) acetate (184 mg,

0.82 mmol). in ethanol (5 mL) was added and the reaction medium was refluxed for 2 h, giving a brown microcrystalline precipitate. The solid material was collected by filtration, washed with cold methanol and diethyl ether (2 × 5 mL), and dried under vacuum. Yield: 405 mg, 83 %. Elemental analysis (%) Calculated $C_{33}H_{30}FeN_2O_5Pd$ (596.88 g mol^{-1}): C, 56.88; H, 4.34; N, 4.02. Found: C, 56.46; H, 4.49; N, 3.94. ESI MS (*m*/*z*) calcd for $C_{33}H_{29}N_2O_5{}^{56}Fe^{106}Pd$: 695.04661, found: 695.0466 $[M - H]^-$. FT-IR (KBr, cm^{-1}): 3429(m) ν(O-H); 3091(w), 3040(m) *ν*(C−H arom); 2934(s), 2925(m), 2858(s) *ν*(C−H aliph); 1680(s) *ν*(C=O), 1607(vs) *ν*(C⋯n); 1576(vs), 1558(vs) *ν*(C⋯O) and/or ν(C⋯C); 1280(m) *ν*(C−O); 737(w)*δ*(C−H). ^{1}H NMR (500 MHz, DMSO-d_6): 9.90 (br s, OH and CO_2H), 7.99 (s, 1 H, N=CH), 7.51 (br d, 1 H, H-6), 7.40 (br d, 1 H, H-3), 7.24 (br d, 2 H, C_6H_4), 7.08 (br d, 1 H, H-5), 6.75 (br d, 2 H, C_6H_4), 5.19 (s, 1 H, CH=C), 4.66 (br s, 2 H, H_α C_5H_4), 4.35 (br s, 2 H, H_β C_5H_4), 4.12 (s, 5 H, C_5H_5), 3.67 (m, 1 H, H-7), 3.64 (m, 1 H, H-8), 2.59 (m, 1 H, H-12b), 2.27 (m, 1 H, H-9b), 1.64 (m, 1 H, H-11b), 1.47 (m, 1 H, H-12a), 1.35 (m, 1 H, H-10b), 1.19 (m, 1 H, H-11a), 0.85 (m, 2 x 1 H, H-9a and H-10a). ^{13}C{^{1}H} NMR (125 MHz, DMSO-d_6): 174.76 (C=O), 164.88 (C-2), 164.40 (CH=*C*), 157.51 (C-OH C_6H_4), 154.95 (N=CH), 131.08 (C_{ipso} C_6H_4), 127.05 (CH C_6H_4), 124.37 (C-6), 121.04 (C-3), 115.37 (CH C_6H_4), 114.53 (C-5), 99.51 (*C*H=C), 81.72 (C_{ipso} C_5H_4), 75.98 (C-7), 69.69 (C-8), 69.55 (C_5H_5 and C_β C_5H_4), 68.05 (C_β C_5H_4), 31.32 (C-9), 27.88 (C-12), 25.08 (C-10), 23.68 (C-11); C-1, C-4 and CO_2H carbons not observed.

X-ray Crystal Structure Determinations

A clear light orange and clear light brown well-shaped single crystal of **3** and **4**·^{i}PrOH, respectively, was mounted on MiTeGen MicroMounts. Diffraction data were collected at 296(2) K on a Bruker D8 QUEST diffractometer equipped with a bidimensional CMOS Photon100 detector, using graphite monochromated Mo-Kα radiation (λ = 0.71073 Å). The diffraction frames were integrated using the APEX2 package,[61] and were corrected for absorptions with SADABS. The solution and refinement for compounds **3** and **4**·^{i}PrOH were carried out with OLEX 2 program.[62] Both structures were solved by direct methods using the ShelXS software.[63] The structures were then refined with full-matrix least-squares methods based on F^2 (ShelXL).[63] All non-hydrogen atoms were refined with anisotropic atomic displacement parameters. All hydrogen atoms were included in their calculated positions, assigned fixed isotropic thermal parameters and constrained to ride on their parent atoms. The isopropanol solvent molecule in **4**·^{i}PrOH has been modeled over two positions with refined

occupancies of 0.58(1) and 0.42(1), the atomic positions of O3, C28, C26 and O3A, C26A, C28 have been set in identical positions using EXYZ constraints. DFIX and DANG instructions were used to restraint the 1,2- and 1,3-distances, respectively, and ISOR instructions were used for atoms C26, C28, C26A, and C28A. Finally, the disordered atoms were constrained to have equivalent anisotropic displacement parameters (EADP instruction). Details about crystal data, collection parameters and refinement are summarized in Table 5, and additional crystallographic details are in the CIF files. ORTEP views were drawn using OLEX2 software.[62]

Table 5 Crystallographic data, details of data collection and structure refinement parameters for compounds **3** and **4**·^{i}PrOH.

Parameters	**3**	**4**·^{i}PrOH
Empirical Formula	$C_{20}H_{26}FeN_2O$	$C_{28}H_{36}FeN_2O_3$
Formula mass, g mol^{-1}	366.28	504.44
Collection T, K	296(2)	296(2)
crystal system	Orthorhombic	orthorhombic
space group	$P2_12_12_1$	$P2_12_12_1$
a (Å)	7.5430(4)	10.2197(6)
b (Å)	8.7848(5)	10.3087(5)
c (Å)	27.6566(16)	25.1548(12)
V (Å^3)	1832.63(18)	2650.1(2)
Z	4	4
D_{calcd} (g cm^{-3})	1.328	1.264
Crystal size (mm)	0.202 × 0.166 × 0.137	0.388 x 0.201 x 0.098
F(000)	776	1072
abs coeff (mm^{-1})	0.831	0.599
θ range (°)	2.433 to 26.404	2.135 to 26.432
range h,k,l	-9/9, -10/10, -34/34	-12/12, -12/12, -31/31
No. total refl.	25642	88090
No. unique refl.	3748	5444
Comp. θ_{max} (%)	100	99.8
Max/min transmission	0.9366/0.8484	0.9668/0.8480
Data/Restraints/Parameters	3758/0/224	5444/36/318
Final R [$I>2\sigma(I)$]	R_1 = 0.0360 wR_2 = 0.0706	R_1 = 0.0378 wR_2 = 0.0976

R indices (all data)	$R_1 = 0.0553$ $wR_2 = 0.0768$	$R_1 = 0.0474$ $wR_2 = 0.1036$
Goodness of fit / F^2	1.062	1.078
Largest diff. Peak/hole ($eÅ^{-3}$)	0.276/-0.176	0.414/-0.266

Computational details

DFT calculations were carried out using the ADF2017 package,[64,65] employing the PBE0 functional[66-68] and the TZ2P basis set,[69] together with Grimme's empirical DFT-D3 corrections for dispersion forces.[70] The optimized geometries were characterized as true minima on the potential energy surface using vibrational frequency calculations (no imaginary values). The UV-vis transitions were calculated by means of TD-DFT calculations on the optimized geometries, at the same level of theory. The graphical SWizard program was used for simulating UV-vis spectra.[71,72]

Author contribution

Conceptualization (D.C. and C.M.), methodology (D. C., C.M. and J.-Y.S.), software (S.C., V.A., M.F. and S.K., validation (D.C., C.M. and J.-R.H.), formal analysis (J.-Y.S. and J.-R.H.), investigation (S.C., P.H., V.A. and S.K.), resources (C.M.), data curation (J.-Y.S. and J.-R.H), writing—original draft preparation (J.-Y.S. and J.-R.H.), writing—review and editing (S.C., C.M., J.-Y.S. and J.-R.H.), supervision (J.-R.H. and C.M.), project administration (C.M.), funding acquisition (D.C., J.-Y.S. and C.M.).

Conflicts of Interest

The authors declare that they have no known competing financial interests or personal relationships that could have appeared to influence the work reported in this paper.

Acknowledgments

We thank S. Sinbandhit (and P. Jehan CRMPO, Rennes) for helpful assistance with NMR and HRMS measurements, respectively. This research was performed as part of the Chilean-French International Research Program "IRP-CoopIC". Financial support from the Fondo Nacional de

Desarrollo Científico y Tecnológico (FONDECYT), Chile (grant 1090310) and FONDEQUIP (EQM130154 and EQM120095), the Vicerrectoría de Investigación y Estudios Avanzados, Pontificia Universidad Católica de Valparaíso, Chile (VRIEA-PUCV), the Centre National de la Recherche Scientifique (CNRS) and the Université de Rennes 1 is gratefully acknowledged. S.C. thanks VRIEA-PUCV and FONDECYT for the postdoctoral financing.

Notes and References

1 T. J. Kealy and P. L. Pauson, *Nature*, 1951, **168**, 1039-1040.

2 S. A. Miller, J. A. Tebboth and J. F. Tremaine, *J. Chem. Soc.*, 1952, 632-635.

3 G. Wilkinson, M. Rosenblum, M. C. Whiting and R. B. Woodward, *J. Am. Chem. Soc.*, 1952, **74**, 2125-2126.

4 E. O. Fischer and W. Pfab, *Z. Naturforsch. B*, 1952, **7**, 377-379.

5 J. D. Dunitz and L. E. Orgel, *Nature*, 1953, **171**, 121-122.

6 D. Astruc, *Eur. J. Inorg. Chem.*, 2017, 6-29.

7 Special Issue: The Multifaceted Chemistry of Ferrocene, P. Stepnicka (Ed.), *Eur. J. Inorg. Chem.*, 2017, January 10, Pp. 212-526.

8 Special issue: Ferrocene: beauty and function, K. Heinze and H. Lang (Eds.), *Organometallics*, 2013, **32**, Issue 20, Pp. 5623-6146.

9 Special issue: R. D. Adams (Ed.), *J. Organomet. Chem.*, 2001, **637–639**, pp. 1-875.

10 E. Lerayer, L. Radal, T. Anh Nguyen, N. Dwadnia, H. Cattey, R. Amardeil, N. Pirio, J. Roger and J.-C. Hierso, *Eur. J. Inorg. Chem.*, 2020, 419-445.

11 (*a*) I. R. Butler, *Organometallics* 2021, **40**, 3240-3244; (*b*) W. Erb, N. Richy, J.-P. Hurvois, P. J. Low and F. Mongin, *Dalton Trans.*, 2021, **50**, 16933-16938.

12 M. Malischewski, M. Adelhardt, J. Sutter, K. Meyer and K. Seppelt, *Science*, 2016, **353**, 678-682.

13 C. A. P. Goodwin, M. J. Giansiracusa, S. M. Greer, H. M. Nicholas, P. Evans, M. Vonci, S. Hill, N. F. Chilton and D. P. Mills, *Nat. Chem.*, 2021, **13**, 243-248.

14 N. Dwadnia, J. Roger, N. Pirio, H. Cattey and J.-C. Hierso, *Coord. Chem. Rev.*, 2018, **355**, 74-100.

15 S. K. Sahoo, *Dalton Trans.*, 2021, **50**, 11681-11700.

16 A. Pal, S. Ranjan Bhatta and A. Thakur, *Coord. Chem. Rev.*, 2021, **431**, 213685.

17 S. M. Beladi-Mousavi, S. Sadaf, A.-K. Hennecke, J. Klein, A. M. Mahmood, C. Rüttiger, M. Gallei, F. Fu, E. Fouquet, J. Ruiz, D. Astruc and L. Walder, The *Angew. Chem. Int. Ed.*, 2021, **60**, 13554-13558.

18 C. Ornelas, *New J. Chem.*, 2011, **35**, 1973-1985.

19 M. Patra and G. Gasser, *Nat. Rev. Chem.*, 2017, **1**, 0066.

20 A. Vessières, Y. Wang, M. J. McGlinchey and G. Jaouen, *Coord. Chem. Rev.*, 2021, **430**, 213658.

21 G. Perli, Q. Wang, C. B. Braga, D. L. Bertuzzi, L. A. Fontana, M. C. P. Soares, J. Ruiz, J. D. Megiatto Jr., D. Astruc and C. Ornelas, *J. Am. Chem. Soc.*, 2021, **143**, 12948-12954.

22 X. Liu, C. Manzur, N. Novoa, S. Celedón, D. Carrillo and J.-R. Hamon, *Coord. Chem. Rev.*, 2018, **357**, 144-172.

23 S. Kaur, M. Kaur, P. Kaur, K. Clays and K. Singh, *Coord. Chem. Rev.*, 2017, **343**, 185-219.

24 M. Malaun, Z. R. Reeves, R. L. Paul, J. C. Jeffery, J. A. McCleverty, M. D. Ward, I. Asselberghs, K. Clays and A. Persoons, *Chem. Commun.*, 2001, 49-50.

25 N. Novoa, C. Manzur, T. Roisnel, V. Dorcet, N. Cabon, F. Robin-Le Guen, I. Ledoux-Rak, S. Kahlal, J.-Y. Saillard, D. Carrillo and J.-R. Hamon, *New J. Chem.*, 2019, **43**, 10468-10481.

26 W. Qin, S. Long, M. Panunzio and S. Biondi, *Molecules*, 2013, **18**, 12264-12289.

27 L. Fabbrizzi, *J. Org. Chem.*, 2020, **85**, 12212-12226.

28 P.A. Vigato and S. Tamburini, *Coord. Chem. Rev.*, 2004, **248**, 1717-2128.

29 K. T. Hylland, I. Gerz, S. DWragg, S. Oien-Odegaard and M. Tilset, *Eur. J. Inorg. Chem.*, 2021, 1869-1889.

30 X. Liu and J.-R. Hamon, *Coord. Chem. Rev.*, 2019, **389**, 94-118.

31 P. Das and W. Linert, Schiff *Coord. Chem. Rev.*, 2016, **311**, 1-23.

32 O. Santoro, X. Zhang and C. Redshaw, *Catalysts*, 2020, **10**, 800.

33 E. Schulz, *Chem. Rec.*, 2021, **21**, 427-439.

34 D. Udhayakumari and V. Inbaraj, *J. Fluorescence*, 2020, **30**, 1203-1223.

35 S. Di Bella, *Dalton Trans.*, 2021, **50**, 6050-6063.

36 D. M. González, L. A. Hernández, J. Oyarce, A. Alfaro, N. Novoa, J. Cisterna, I. Brito, D. Carrillo and C. Manzur, *Synth. Met.*, 2021, **271**, 116633.

37 L. Rigamonti, A. Forni, E. Cariati, G. Malavasi and A. Pasini, *Materials*, 2019, **12**, 3595.

38 E. David, A. Colombo, C. Dragonetti and N. Palanisami, *Chem. Eur. J.*, 2021, **27**, 7124-7137.

39 S. Celedón, T. Roisnel, V. Artigas, M. Fuentealba, D. Carrillo, I. Ledoux-Rak, J.-R. Hamon and C. Manzur, *New J. Chem.*, 2020, **44,** 9190-9201.

40 M. S. Hossain, P. K. Roy, C. Zakaria and M. Kudrat-E-Zahan, *Int. J. Chem. Stud.*, 2018, **6**, 19-31.

41 L. Rigamonti, F. Reginato, E. Ferrari, L. Pigani, L. Gigli, N. Demitri, P. Kopel, B. Tesarova and Z. Heger, *Dalton Trans.*, 2020, **49**, 14626-14639.

42 Y. Lin, H. Betts, S. Keller, K. Cariou and G. Gasser, *Chem. Soc. Rev.*, 2021, **50**, 10346-10402.

43 G. Bett, D. E. Fenton and J. R. Tate, *Inorg. Chim. Acta*, 1981, **54**, L101-L102.

44 A. Trujillo, S. Sinbandhit, L. Toupet, D. Carrillo, C. Manzur and J.-R. Hamon, *J. Inorg. Organomet. Polym. Mater.*, 2008, **18**, 81-99.

45 M. Fuentealba, A. Trujillo, J.-R. Hamon, D. Carrillo and C. Manzur, *J. Mol. Struct.*, 2008, **881**, 76-82.

46 S. Celedón, M. Fuentealba, T. Roisnel, J.-R. Hamon, D. Carrillo and C. Manzur, *Inorg. Chim. Acta*, 2012, **390**, 184-189.

47 G. Lenoble, P. G. Lacroix, J.-C. Daran, S. Di Bella and K. Nakatani, *Inorg. Chem.*, 1998, **37**, 2158-2165.

48 F. Averseng, P. G. Lacroix, I. Malfant, F. Dahan and K. Nakatani, *J. Mater. Chem.*, 2000, **10**, 1013-1018.

49 J. V. Greenhill, *Chem. Soc. Rev.*, 1977, **6**, 277-294.

50 J. S. Danilova, S. M. Avdoshenko, M. P. Karushev, A. M. Timonov and E. Dmitrieva, *J. Mol. Struct.*, 2021, **1241**, 130668.

51 S. Celedón, T. Roisnel, D. Carrillo, I. Ledoux-Rak, J.-R. Hamon and C. Manzur, *J. Coord. Chem.*, 2020, **73**, 3079-3094.

52 S. Celedón, M. Fuentealba, T. Roisnel, I. Ledoux-Rak, J.-R. Hamon, D. Carrillo and C. Manzur, *Eur. J. Inorg. Chem.*, 2016, 3012-3023.

53 P. Gilli, V. Bertolasi, V. Ferretti and G. Gilli, *J. Am. Chem. Soc.*, 2000, **122**, 10405-10417.

54 R. Taylor and P. A. Wood, *Chem. Rev.*, 2019, **119**, 9427-9477.

55 N. Novoa, T. Roisnel, P. Hamon, S. Kahlal, C. Manzur, H. M. Ngo, I. Ledoux-Rak, J.-Y. Saillard, D. Carrillo and J.-R. Hamon, *Dalton Trans.*, 2015, **44**, 18019-18037.

56 S. Di Bella, *Chem. Soc. Rev.*, 2001, **30**, 355-366.

57 P. Zanello, Electrochemical and X-ray Structural Aspects of Transition Metal Complexes Containing Redox-Active Ferrocene Ligands, in Ferrocenes: Homogeneous Catalysis, Organic Synthesis, Materials Science, A. Togni and T. Hayashi (Eds.), VCH, New York, 1995, Ch 7, pp. 317-430.

58 L. Yang, D. R. Powell and R. P. Houser, *Dalton Trans.*, 2007, 955–964.

59 W.L.F. Armarego and C.L.L. Chai, Purification of Laboratory Chemicals, 5th ed.; Butterworth-Heinemann, Elsevier Inc.: Amsterdam, The Netherlands, 2003.

60 M. Fuentealba, J.-R. Hamon, D. Carrillo and C. Manzur, *New J. Chem.*, 2007, **31**, 1815-1825.

61 APEX2, Bruker AXS Inc., Madison, Wisconsin, USA, 2007.

62 O.V. Dolomanov, L.J. Bourhis, R.J. Gildea, J.A.K. Howard and H. Puschmann, *J. Appl. Crystallogr.*, 2009, **42**, 339-341.

63 G.M. Sheldrick,. *Acta Crystallogr., Sect. C Struct. Chem.*, 2015, **71**, 3-8.

64 G. te Velde, F. M. Bickelhaupt, E. J. Baerends, C. Fonseca Guerra, S. J. A. van Gisbergen, J. G. Snijders and T. Ziegler, *J. Comput. Chem.*, 2001, **22**, 931-967.

65 ADF 2021.1, SCM, Theoretical Chemistry, Vrije Universiteit, Amsterdam, The Netherlands, http://www.scm.com.

66 J. P. Perdew, K. Burke and M. Ernzerhof, *Phys. Rev. Lett.*, 1996, **77**, 3865-3868.

67 J. P. Perdew, K. Burke and M. Ernzerhof, *Phys. Rev. Lett.*, 1997, **78**, 1396-1396.

68 C. Adamo and V. Barone, *J. Chem. Phys.*, 1999, **110**, 6158-6170.

69 E. Van Lenthe and E. J. Baerends, *J. Comput. Chem.*, 2003, **24**, 1142-1156.

70 S. Grimme, S. Ehrlich and L. Goerigk, *J. Comput. Chem.*, 2011, **32**, 1456-1465.

71 S. I. Gorelsky, SWizard program, http://www.sg-chem.net/, University of Ottawa, Ottawa, Canada, 2013.

72 S. I. Gorelsky and A. B. P. Lever, *J. Organomet. Chem.*, 2001, **635**, 187-196.